7.5

OCEAN SURFACE ROUGHNESS SPECTRUM AND MICROWAVE BRIGHTNESS TEMPERATURE

Paul A. Hwang,[1*] Derek M. Burrage,[2] David W.-C. Wang,[2] and Joel C. Wesson[2]
[1]Remote Sensing Division, Naval Research Laboratory, Washington DC
[2]Oceanography Division, Naval Research Laboratory, Stennis Space Center, MS

1. INTRODUCTION

After a long period of planning and development, global remote sensing of sea surface salinity (SSS) from space is becoming a reality with the launch of SMOS (Soil Moisture and Ocean Salinity) satellite by the European Space Agency (ESA) in November 2009 (Font et al. 2010). A similar mission (AQUARIUS/SAC-D), jointly sponsored by the United States National Aeronautics and Space Administration (NASA) and Argentine Space Agency, CONAE, is scheduled for launch later this year. The microwave L band centered on 1.413 GHz and with a bandwidth of 25 MHz is selected for soil moisture and ocean salinity retrievals because this frequency band is protected for use by radio astronomy. For this band, it has been determined that the ocean surface roughness is the leading geophysical error source for sea surface salinity retrieval (Lagerloef et al. 2008).

The spectrum of ocean surface roughness relevant to microwave remote sensing remains poorly defined. Many roughness models have been published but very few intercomparison studies reported. The difficulty of specifying an optimal roughness spectrum is highlighted in the comparison between field measurements and analytical computations. For example, Yueh (1997) selects Durden and Vesecky (1985), denoted DV, for his two-scale model computation but finds it necessary to double the roughness spectral densities in order to obtain a reasonable agreement with field measurements. Camps et al. (2004) use the spectrum models of Durden and Vesecky (1985) and Elfouhaily et al. (1997) and also have to double the roughness spectral densities of both models to achieve approximate agreement between calculated and measured wind speed sensitivity of brightness temperature.

Similar difficulty of specifying the ocean surface roughness spectrum is also encountered in active radar scattering computations. In a recent study, Hwang and Plant (2010) present a comparison study of calculated normalized radar cross sections (NRCS) using three spectrum models: Donelan-Banner-Plant (Plant 2002), Elfouhaily et al. (1997), and Hwang (2008), abbreviated as D, E, and H, respectively. The H spectrum is constructed from the parameterization function of field measurements of short scale surface waves (wavelengths between 0.02 and 6 m or wave number k between 1 and 300 rad/m) (Hwang and Wang 2004; Hwang 2005) following the analysis of source term balance by Phillips (1984). Analytical expressions are de-

veloped to extend the wave number coverage to longer and shorter wave components outside the measured spectral range (Hwang 2008, 2010). (The H spectrum model uses the directional distribution function of the D model.) The computed NRCS are compared to field data of NRCS measurements covering microwave frequencies from 1 to 18 GHz as well as Ku and C band geophysical model functions (GMF). Briefly, the results illustrate the significant differences in the spectral representation of the ocean surface roughness and the low-passed mean square slopes (MSS) among different spectrum models. The low-passed MSS integrating the three roughness spectrum models over several bandwidths are compared to available field data obtained through remote sensing using electromagnetic (EM) frequencies ranging from optical (Cox and Munk 1954) to microwave at Ka band (36 GHz) (Walsh et al. 1998; Vandemark et al. 2004), Ku band (14 GHz) (Jackson et al. 1992; Jones et al. 1977; Wentz 1977) and C band (5.3 GHz) (Hauser et al. 2008). The D spectrum yields good agreement with the low-passed MSS of wave components longer than about 0.3 m but underpredicts the MSS of shorter wavelength bands. The E spectrum produces good agreement for both high and low ends of the integrating wavelength range, but underpredicts the intermediate length scales for wind speeds higher than about 7 m/s. The H spectrum gives an overall better agreement with field measurements across all wavelength bands (Hwang and Plant 2010, Figure 2). The computed Ku band NRCS is sensitive to the selected roughness spectrum. The D spectrum performs very well for VV (vertical transmit and vertical receive) polarization but less accurately for HH (horizontal transmit and horizontal receive) polarization. The E spectrum performs well for HH polarization but is less accurate for VV polarization. The H spectrum produces more even agreement for VV and HH, and thus a better result on the VV/HH polarization ratio. The computed C band NRCS is much less sensitive to the choice of roughness spectrum and the agreement between NRCS computations and GMF is generally much better than the corresponding comparison of Ku band results for wind speed, U_{10}, between 3 and 24 m/s and incidence angle, θ, between 20° and 60°. The NRCS comparison study indicates that further improvement is needed for wave components in the centimeter region (Hwang 2010).

In this paper, we report brightness temperature computations using four different models of the ocean surface roughness spectrum: the D, E and H spectra mentioned in the last paragraph plus Kudryavtsev et al. (1999), denoted the K spectrum. The EM model of microwave brightness temperature, T_B, is based on the small slope approximation (SSA) and the small perturbation method (SPM) for solving the Maxwell's equa-

Corresponding author address: Paul A. Hwang, Remote Sensing Division, Naval Research Laboratory, 4555 Overlook Avenue SW 20375.
Email: paul.hwang@nrl.navy.mil

tions, and denoted SPM/SSA. The theoretical aspects of the EM model have been described in great detail by Yueh et al. (1994a, b) and Johnson and Zhang (1999). Irisov (1997) has shown that the surface emissivity computation based on the SPM produces a solution that can be expressed as a series of surface slope instead of surface height, so the SPM solution of microwave emission remains accurate for ocean applications even when it fails for the corresponding radar scattering calculations. The SPM/SSA EM model coupled with the K spectrum is one of three alternative roughness correction models used in the SMOS processing chain. The others, not discussed here, are the two-scale model of Yueh (1997) and an empirical multi-parameter retrieval model (Gabarro et al. 2004; Etcheto et al. 2004).

Section 2 presents analyses and discussions of the four ocean surface roughness spectrum models, brightness temperature computation, and comparisons of computed results with data from two field experiments of brightness temperature measurements conducted on instrumented towers (Hollinger 1971; Camps et al. 2004), and Section 3 is a summary.

2. ANALYSIS

2.1. Surface roughness spectrum

In active remote sensing, the dominant backscattering mechanism is Bragg resonance. The secondary mechanism is the modification of local incidence angle caused by the longer waves tilting the Bragg resonance surface roughness components. In passive remote sensing, the situation is more complex. The two modes of remote sensing are connected through the Kirchhoff's law relating the emissivity and reflectivity of the medium (emissivity = 1 − reflectivity); for emissivity computation, the reflectivity is an integral over the upper hemisphere of the bistatic scattering coefficients in the reciprocal active scattering problem. The surface roughness contributing to passive remote sensing thus covers a much wider spectral band than it does in the active mode. From detailed analyses presented by Yueh et al. (1994a, b) and Johnson and Zhang (1999), the roughness contribution to the surface emissivity can be treated as the product of an electromagnetic weighting function and the surface roughness spectrum. The weighting function shows resonance peaks in the neighborhood of surface wave length scale comparable to the EM wavelength. In this respect, the roughness properties of wave number components in the neighborhood of Bragg resonance and EM wavelength are of great importance to both active and passive remote sensing problems.

Considerable difference is found in the representation of the sea surface roughness spectrum by the four spectrum models under investigation. For example, Figure 1 shows an example of comparison at two wave numbers corresponding approximately to the Bragg resonance wavelengths of L and K microwave frequency bands operated in moderate incidence angles (about 25° to 60°). The spectral density is expressed in directionally integrated dimensionless form,

$B(k) = \int_{-\pi}^{\pi} k^4 W(k,\phi)d\phi$, where W is the directional spectrum of ocean surface elevation and ϕ wave propagation direction with respect to the wind. The E spectrum displays a non-monotonic wind speed dependence. For comparison, the DV spectrum is also displayed. The short scale waves in the DV spectrum is based on the outdated concept of a saturation range and log(k) wind-speed dependence of high-frequency surface waves. More recent research of wind generated waves shows a more complex wind speed dependence ranging from approximately linear for meter-scale waves, decreasing to less than linear for decimeter waves, then increasing to approximately cubic for sub-centimeter waves as a consequence of wave breaking contribution (Hwang and Wang 2004; Hwang 2010), as reflected in the wind speed dependence of radar backscatter from the ocean surface, see results summarized by Hwang (1997).

Interestingly, the spectral density around the L band resonance component in the H spectrum is about twice that of the E spectrum for U_{10} higher than about 5 m/s (Figure 1a). As discussed in the Introduction section, Camps et al. (2004) found it necessary to double the E spectrum to obtain reasonable agreement between the computed rate of change of brightness temperature with wind speed and the corresponding L band field measurements. Using the H spectrum, the artificial doubling can be avoided.
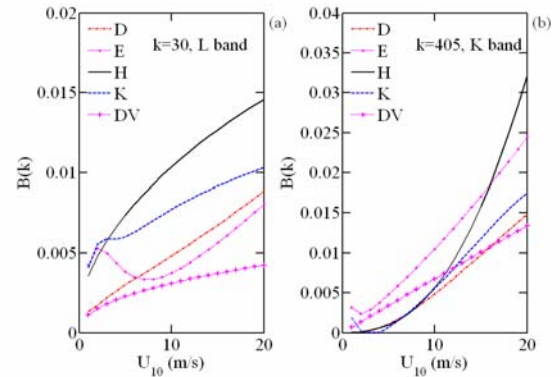
Figure 1. Dimensionless spectral densities at k=30 and 405 rad/m, corresponding approximately to those of the Bragg resonance waves of L and K microwave frequency bands operated at incidence angles of about 30°. Results from D, E, H, K and DV spectrum models are shown.

2.2. Microwave brightness temperature computation

Theoretical analysis of the microwave emission is a very complex subject. In addition to the ocean surface emission, atmospheric upwelling, reflection of the atmospheric downwelling, and frequency-dependent contributions from whitecaps can all introduce considerable complication in the received microwave signal. There have been many papers published on these complicated subjects. For the computation of ocean surface emission, the two scale model (e.g., Wentz 1977; Yueh 19997; Johnson 2006; Lyzenga 2006) and SPM/SSA

(Yueh et al., 1994a, b; Johnson and Zhang 1999) are frequently used. Lyzenga (2006) finds that the results from the two models are not very different. Here, we choose the SSA/SPM model (Johnson and Zhang 1999), as implemented in MATLAB code (Reul and Chapron 2001, 2003) and used in SMOS L2 processing, for our investigation of the roughness effect on the microwave brightness temperature computation.

The brightness temperature, T_B, of horizontal and vertical polarizations at microwave frequency, f, incidence angle, θ, and azimuth angle (with respect to the wind direction), ϕ, can be expressed as (Johnson and Zhang 1999; Reul and Chapron 2001, 2003)

$$\begin{bmatrix} T_{BH}(f,\theta,\phi) \\ T_{BV}(f,\theta,\phi) \end{bmatrix} = T_s \left\{ \begin{bmatrix} 1 - \left|R_{HH}^{(0)}\right|^2 \\ 1 - \left|R_{VV}^{(0)}\right|^2 \end{bmatrix} - \begin{bmatrix} \Delta e_{BH} \\ \Delta e_{BV} \end{bmatrix} \right\}, \quad (1)$$

where T_s is the sea surface temperature (SST), $R_{pp}^{(0)}(f,\theta)$ the Fresnel reflection coefficient of p polarization, and $\Delta e_{Bp}(f,\theta,\phi)$ the emissivity change due to the rough sea surface. (For simplicity, we have used "incidence angle" to represent the polar or zenith angle of observation for both passive and active systems in this paper.) The first term on the right hand side of (1) represents the solution for the brightness temperature of a flat sea surface. The contribution from a rough sea is evaluated from the second term through the roughness-induced emissivity change, which can be written as (Johnson and Zhang 1999)

$$\begin{bmatrix} \Delta e_{BH} \\ \Delta e_{BV} \end{bmatrix} = \int_0^\infty \int_{-\pi}^{\pi} W(k',\phi') \begin{bmatrix} g_H(f,\theta,\phi,\varepsilon_{sw},k',\phi') \\ g_V(f,\theta,\phi,\varepsilon_{sw},k',\phi') \end{bmatrix} k'd\phi'dk', (2)$$

where ε_{sw} is the sea water dielectric constant, and g_p the electromagnetic "weighting" function for the p polarization, the full expression of which is given in Johnson and Zhang (1999, p. 2308) and Yueh et al. (1994a, Appendices 1-3).

The emissivity change can be expressed in azimuthal harmonic terms (Yueh et al. 1994b). To the second order small slope approximation, only the even terms up to the second harmonics can be resolved (Johnson and Zhang 1999; Reul and Chapron 2003) and

$$\Delta e_{Bp} = \Delta e_{Bp}^{(0)} + \Delta e_{Bp}^{(2)} \cos(2\phi). \quad (3)$$

where

$$\Delta e_{Bp}^{(0)} = \int_0^\infty B_0(k_r\beta) g_{p,0}'(\beta) d\beta, \quad (4)$$

$$\Delta e_{Bp}^{(2)} = 2\int_0^\infty B_2(k_r\beta) \mathrm{Re}\{g_{p,2}'(\beta)\} d\beta, \quad (5)$$

B_n is the n-th azimuthal harmonic of the dimensionless surface roughness spectrum, $B(k,\phi) = k^4 W(k,\phi)$, $\beta{=}k/k_r$, k_r the electromagnetic wavenumber, and $g_{p,n}'$ the n-th azimuthal harmonic of the rescaled weighting function, g_p' (Johnson and Zhang 1999),

$$g_p'(\theta,\phi,\varepsilon_{sw},\beta,\phi')d\beta = \frac{1}{k^3}\left[g_p(f,\theta,\phi,\varepsilon_{sw},k,\phi')\right]dk. \quad (6)$$

SPM/SSA computations of T_B for 1.41, 8.36 and 19.34 GHz (L, X, and K bands, respectively) are performed using the four roughness models for incidence angles ranging between 0° and 70° in 5° or 10° steps and wind speeds ranging between 2 and 14 m/s in 2 m/s steps (the flat surface solution corresponds to 0 m/s wind). The spectrum is calculated with 128 wave number components spaced logarithmically within the range from 0.01 to 4024 rad/m, and 128 directional components (the azimuthal resolution is 2.8°). The sea surface salinity (SSS) is 35 psu and sea surface temperature (SST) 18°C (291 K). The upper limit of the normalized wave number, β_{max}, for the integration of weighting function in (4) and (5) is fixed at 128 or $4024/k_r$. Thus, for the three microwave frequencies of 1.41, 8.36 and 19.34 GHz, β_{max} = 128, 22.9 and 9.9, respectively. From numerical experimenting, the computational results vary somewhat with the value of β_{max}. Figure 2 presents an example of the calculated brightness temperature, T_B, and the surface roughness induced component, $\Delta T_B = T_s\Delta e_B$, based on β_{max} = 2, 4, 16 and 128 for the L band microwave frequency (1.41 GHz). For clarity of presentation, only the results using the H spectrum are displayed.
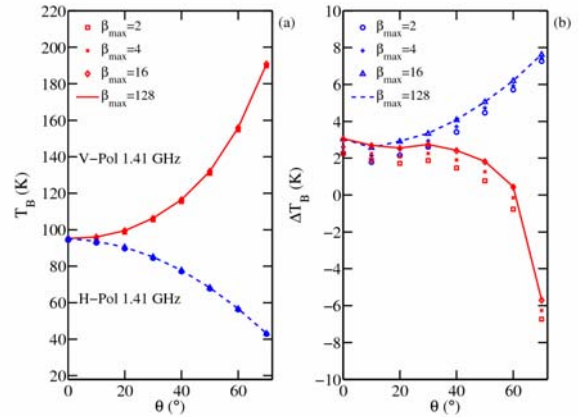
Figure 2. An example of the L band (1.41 GHz) (a) T_B, and (b) ΔT_B, calculated with different bandwidths of the ocean surface wave spectrum for U_{10} = 10 m/s. Illustrated here are the results of H spectrum for β_{max} = 2, 4, 16 and 128.

Similarly, Figure 3 shows the results of ΔT_{BH} calculated with β_{max} = 16 and 128 for 1.41 GHz, 2 and 16 for 8.36 GHz, and 2 and 9.9 for 19.34 GHz. For clarity of presentation, only the results of H and E spectra are shown. The wind speed for these examples is U_{10} = 10 m/s. Based on these numerical experiments, for sea surface emission computation with L band or higher microwave frequencies, the integration limit of the surface roughness spectrum can be set at about k_{max} = 500 rad/m or β_{max} somewhat higher than 2, whichever results in the higher wave number. This is consistent with the behavior of the weighting function, which shows resonance peaks in the neighborhood of the surface wave number corresponding to the EM wavelength, and a

sharp dropoff toward short scale wave components (e.g., see Figures 1 to 3 of Johnson and Zhang (1999)). To be conservative, however, the results presented in the next section is based on k_{max} = 4024 rad/m for X and K bands (β_{max} = 22.9 and 9.9, respectively) and 3780 rad/m for L band (β_{max} = 128). Further discussions on T_B, its rate of change with wind speed, $\partial T_B/\partial U_{10}$, and their comparison with field data are presented in the next section.

2.3. Comparison with field data

Hollinger (1971) presents passive microwave measurements from Argus Island tower (approximately 45 km southwest of Bermuda with 60 m local water depth) at 1.41, 8.36 and 19.34 GHz. The sea foam contribution is removed through post processing. The reported data include T_B measurements of vertical and horizontal polarizations (SSS 35±1 psu, SST 291±1 K) for $U_{43.3}$ = 0.5 and 13.5 m/s, where $U_{43.3}$ is wind speed at 43.3 m above the mean sea level. Applying the logarithmic wind speed profile, for dynamic roughness of 10^{-5} to 10^{-3} m $U_{43.3}$ = (1.12 to 1.16) U_{10}. The results show a definite frequency-dependent correlation between the microwave brightness temperature and wind speed; the correlation is attributed to the effects of wind-induced ocean surface roughness.
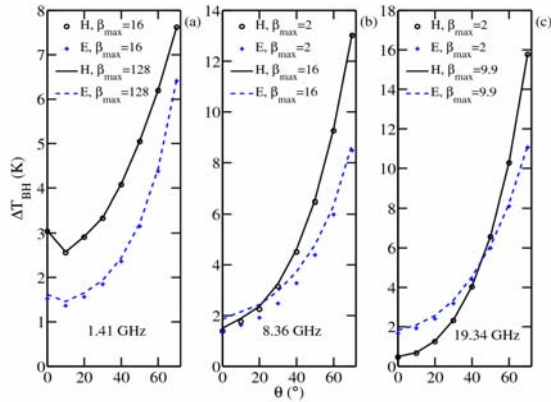
Figure 3. An example of ΔT_{BH} calculated with different bandwidths of the ocean surface wave spectrum for U_{10} = 10 m/s. Illustrated here are the results of E and H spectra for (a) β_{max} = 16 and 128 (1.41 GHz), (b) β_{max} = 2 and 16 (8.36 GHz), and (c) β_{max} = 2 and 9.9 (19.34 GHz).

The field data are displayed in Figure 4. Superimposed in the figure are the computed curves for U_{10} = 0 and 12 m/s (accounting for the factor of $U_{43.3} \approx 1.14\ U_{10}$) for comparison with data. In the plotted scale showing the full range of data, all four models of the ocean surface roughness spectrum produce results in similar agreement with the field measurements. In general, the calculated results compare well with field data but somewhat larger differences are found in the 1.41 GHz case. The L band data of Hollinger (1971) may have an absolute calibration problem or a radiometer bias as

noted in the personal communications with Swift (1974, p. 648) and Wentz (1975, p. 3443).

The degrading of agreement between computations and measurements toward higher microwave frequency is also observed in the comparison analysis of active radar backscattering cross section. Hwang and Plant (2010) have shown that the overall difference between computations and measurements is usually larger in Ku band (14 GHz) than in C band (5.3 GHz). Furthermore, the NRCS calculated for Ku band is more sensitive to the selection of roughness model than that for C band. The NRCS analysis has lead to an adjustment of the empirical parameterization of the H spectrum (Hwang 2010).
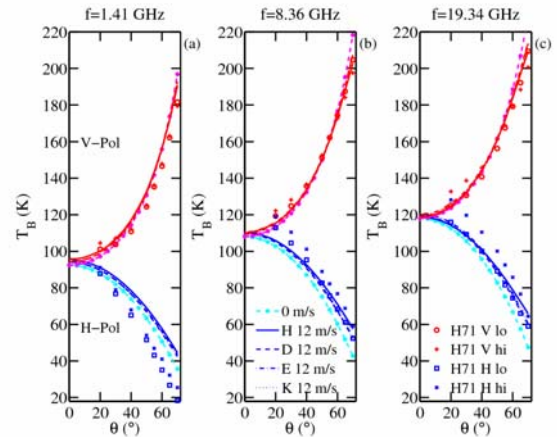
Figure 4. Brightness temperatures at (a) 1.41 GHz, (b) 8.36 GHz, and (c) 19.34 GHz microwave frequencies, calculated with four different spectrum models of the ocean surface roughness for U_{10} = 0 and 12 m/s. The field data ($U_{43.3}$ = 0.5 and 13.5 m/s) reported by Hollinger (1971) (abbreviated as H71 in the legend) are superimposed for comparison; the factor of $U_{43.3} \approx 1.14\ U_{10}$ is applied.

Hollinger (1971) processes his data to obtain the rate of change of T_B with respect to wind speed at different incidence angles. This processing method is also adopted by Camps et al. (2004) for their L band radiometer measurements (1.413 GHz, SSS about 38 psu, and SST about 280 to 295 K). For the horizontal polarization, the increasing trend of T_B with wind speed is conspicuous but the data scatter is much larger in the vertical polarization results (e.g., Camps et al. (2004, Figure 6); Etcheto et al. (2004, Figure 8)). Figure 5 shows the computed wind sensitivity, $\partial T_B/\partial U_{10}$ at 1.41, 8.36 and 19.34 GHz. The field measurements reported by Hollinger (1971) and Camps et al. (2004) are superimposed. The computed $\partial T_B/\partial U_{10}$ is very sensitive to the choice of ocean surface roughness model and a factor-of-two difference is common. For the horizontal polarization, the E spectrum underestimates the sensitivity by a factor of about two with respect to the Camps et al. 1.41 GHz data, as discussed in section 2. A similar level of underestimation is also found in the comparison of D, E and K spectrum with Hollinger data at 19.34 GHz. The H

spectrum calculated wind sea (H1) and moderate swell condition (H3) are in good agreement with field data.

We note that in the common frequency (1.41 GHz), the two data sets differ considerably, especially for incidence angles less than about 50°. In particular, the magnitude of V-pol $\partial T_B/\partial U_{10}$ of the former is significantly smaller than that of the latter, while the opposite is true for the H-pol. As discussed by Camps et al. (2004, p. 813-814), a possible source of discrepancy lies in their data being derived mostly from mild to moderate wind conditions, with nearly half of the measurements being performed with wind speeds under 5 m/s and only about one-fifth at speeds above 10 m/s, so that errors in the computed sensitivities at low winds likely dominate the weighted average. They also noted possible influence of wave reflection and destructive interference on data acquired at certain incidence angles from their observational platform on the Casablanca oil rig.
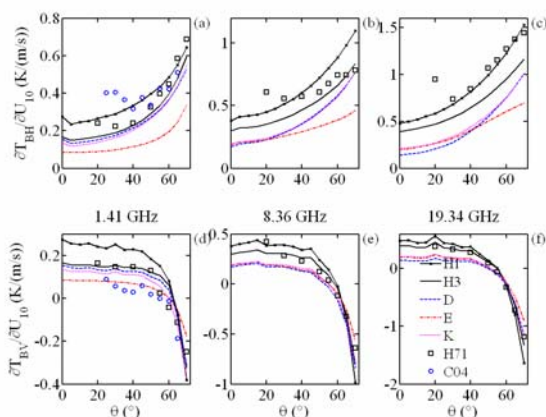
Fig. 5. Wind speed sensitivity, $\partial T_B/\partial U_{10}$, at 1.41, 8.36 and 19.34 GHz calculated with spectrum models D, E, K and H, as a function of incidence angle. Results are averaged over the wind speed range of 2-14 m/s for H-pol (upper panels) and V-pol (lower panels). Field data from Hollinger (1971) (H71) and Camps et al. (2004) (C04) are superimposed. The H spectrum includes a swell index: H1 for wind sea and H3 for moderate swell.

Fig. 6 shows the wind-induced sea surface emissivity, expressed in terms of the brightness temperature change, from WindSat measurements GHz of wind storms at 6, 10, 18 23 and 37 GHz [24]. The results are compared to the SSA/SPM computations with D, E, H and K spectra. Mild swell condition is assumed for the H spectrum (denoted H2).The nominal values of the incidence angles of WindSat frequency channels vary from about 50° to 55° and the computational results are the average of the two angles. The agreement between measurements and computation with the H spectrum is generally very good except at the highest frequency. This is in drastic contrast with the comparison between WindSat measurements and computational results using D, E and K spectra. It is, however, somewhat unsettling that with the H spectrum, the emissivity change can be explained by surface roughness alone, at least to 23 GHz, without invoking contributions from wave breaking

processes such as whitecaps and foam. It is emphasized that for V-pol radar scattering computation, of which wave breaking can usually be ignored, the H spectrum produces excellent agreement with C and Ku band GMF, which in turn are shown to be in very good agreement with field measurements (Hwang 2010). We feel that the clarification of ocean surface spectrum issues is critical to the assessment of breaking and whitecap contributions to brightness temperature measurements in the open ocean.
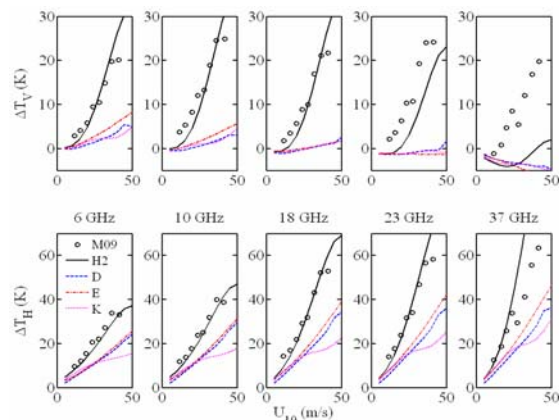
Fig. 6. Change of brightness temperature due to wind-induced ocean surface roughness from WindSat global measurements [24] and comparison with the computations with D, E, H and K spectrum models.

d. Discussion

Accurate specification of the ocean surface roughness spectrum is important to the understanding of many upper ocean processes related to air-sea interaction. Examples relevant to active and pass microwave remote sensing include ocean surface wind stress and wind wave generation mechanisms. It is clear that deficiencies exist in all published models of ocean surface roughness spectrum. Refinement of the ocean surface roughness models requires better approaches than a simple multiplication of the spectral densities across all frequencies by some factor. Because measurements of short scale waves important to microwave remote sensing, ranging from several millimeters to several meters long, using in situ sensors remain a difficult challenge, inversion of remote sensing data to recover the sea surface roughness spectrum is more likely to succeed in acquiring the sea truth. The ocean surface roughness information is also important to understanding of air-sea interaction processes, such as gas transfer and wind wave generation. A systematic analysis of how different spectrum models perform in active and passive microwave computations will be helpful for improving the spectrum models of ocean surface roughness.

3. SUMMARY

In this paper, we investigate the effect of different models of ocean surface roughness spectrum on microwave brightness temperature computation. Four

spectrum models, D (Plant 2002), E (Elfouhaily et al., 1997; Plant 2002), H (Hwang 2008, 2010) and K (Kudryavtsev et al. 1999), are compared. The results show significant differences in the spectral representation of the ocean surface roughness among different models (Figure 1). Based on comparison with low-passed MSS data measured by optical sensing and microwave radars operated at Ka, Ku and C frequency bands, the H spectrum provides the most realistic representation of the ocean surface roughness (Hwang and Plant, 2010, Section 2).

The difference in the spectral representation of ocean surface roughness is reflected in the computed surface roughness induced brightness temperature changes, ΔT_B, and wind speed sensitivity, $\partial T_B/\partial U_{10}$. The calculated values using the four spectrum models can differ by a factor of about two (Figure 5). All four spectrum models show different degrees of agreement and disagreement with field data (Hollinger 1971; Camps et al. 2004). In terms of ΔT_B and $\partial T_B/\partial U_{10}$, the H spectrum gives a better overall agreement with field data. There are still considerable difficulties in reconciling active or passive microwave computations with field measurements, as well as reconciling the differences among different field data sets. A better understanding of the differences between computations and field measurements may provide useful guidelines for future refinement of spectrum models of ocean surface roughness. Improvements of roughness models may lead to more accurate calculations of radar cross section and ocean surface emissivity as well as quality enhancement of retrieved geophysical parameters from EM remote sensing, such as sea surface wind fields, temperature and salinity.

ACKNOWLEDGEMENTS

REFERENCES

Apel, J. R., 2004: An improved model of the ocean surface-wave vector spectrum and its effects on radar backscatter. *J. Geophys. Res.,* 99, 16269-16291.

Camps, A., et al., 2004: The WISE 2000 and 2001 field experiments in support of the SMOS Mission: Sea surface L-band brightness temperature observations and their application to sea surface salinity retrieval. *IEEE Trans. Geos. Remote Sens.,* 42, 804-823.

Durden, S. L., and J. F. Vesecky, 1985: A physical radar cross-section model for a wind-driven sea with swell. *IEEE J. Oceanic Eng.,* 10, 445–451.

Elfouhaily, T., B. Chapron, K. Katsaros, and D. Vandemark, 1987: A unified directional spectrum for long and short wind-driven waves. *J. Geophys. Res.,* 102, 15781-15796.

Etcheto, J., E. P. Dinnat, J. Boutin, A. Camps, J. Miller, S. Contardo, J. Wesson, J. Font, and G. Long, 2004: Wind speed effect on L-band brightness temperature inferred from EuroSTARRS and WISE 2001 field experiments. *IEEE Trans. Geos. Remote Sens.,* 42, 2206-2213.

Font, J., A. Camps, A. Borges, M. Martin-Neira, J. Boutin, N. Reul, Y. H. Kerr, A. Hahne, and S. Meckelenburg, 2010: SMOS: The challenging sea surface salinity measurement from space. *IEEE Proc.,* 98, 649-665.

Gabarro, C., J. Font, A. Camps, M. Vall-llosera, and A. Julia, 2004: new empirical model for microwave sea surface microwave emissivity for salinity remote sensing. *Geophys. Res. Lett.,* 31, L01309.

Hauser, D., G. Caudal, S. Guimbard, and A. A. Mouche, 2008: A study of the slope probability density function of the ocean waves from radar observations. *J. Geophys. Res.*, 113, C02006, doi:10.1029/ 2007JC004264.

Hollinger, J. P., 1971: Passive microwave measurements of sea surface roughness. *IEEE Trans. Geos. Electron.,* 9, 165-169.

Hwang, P. A., 1997: A study of the wavenumber spectra of short water waves in the ocean. Part 2: Spectral model and mean square slope. *J. Atmos. and Oceanic Tech.*, *14*, 1174-1186.

Hwang, P. A., 2005: Wave number spectrum and mean-square slope of intermediate-scale ocean surface waves. *J. Geophys. Res.*, 110, C10029, doi:10.1029/2005JC003002.

Hwang, P. A., 2008: Observations of swell influence on ocean surface roughness. *J. Geophys. Res.,* 113, C12024, doi:10.1029/2008JC005075.

Hwang, P. A., 2010: A note on the ocean surface roughness spectrum. Subm. *J. Atmos. Ocean. Tech.*

Hwang, P. A., and W. J. Plant, 2010: An analysis of the effects of swell and roughness spectra on microwave backscatter from the ocean. *J. Geophys. Res.*, 115*,* C04014, doi:10.1029/2009JC005558.

Hwang, P. A., and D. W. Wang, 2004: An empirical investigation of source term balance of small scale surface waves. *Geophys. Res. Lett.*, 31, L15301, doi:10.1029/2004GL20080.

Irisov, V. G., 1997: Small-slope expansion for thermal and reflected radiation from a rough surface. *Waves Random Media*, 7, 1–10.

Jackson, F. C., W. T. Walton, D. E. Hines, B. A. Walter, and C. Y. Peng, 1992: Sea surface mean-square slope from K_u-band backscatter data. *J. Geophys. Res.*, 97, 11411-11427.

Johnson, J. T., 2006: An efficient two-scale model for the computation of thermal emission and atmospheric reflection from the sea surface. *IEEE Trans. Geos. Remote Sens.*, 44, 560-568.

Johnson, J. T., and M. Zhang, 1999: Theoretical study of the small slope approximation for ocean polarimetric thermal emission. *IEEE Trans. Geos. Remote Sens.*, 37, 2305-2316.

Jones, W. L., L. C. Schroeder, and K. L. Mitchell, 1977: Aircraft measurements of the microwave scattering signature of the ocean. *J. Ocean. Eng.*, 2, 52-61.

Jones, W. L., and L. C. Schroeder, 1978: Radar backscatter from the ocean: Dependence on surface fric-

tion velocity. *Bound.-Layer Meteorol.*, 13, 133-149.

Klein, L. A., and C. T. Swift, 1977: An improved model for the dielectric constant of sea water at microwave frequencies. *IEEE Trans. Antennas Propag.,* 25, 104-111.

Kudryavtsev, V., V. Makin, and B. Chapron, 1999: Coupled sea surface atmosphere model, 2, Spectrum of short wind waves. *J. Geophys. Res.,* 104, 7625–7639.

Lagerloef, G., R. Colomb, D. Le Vine, F. Wentz, S. Yueh, C. Ruf, J. Lilly, J. Gunn, Y. Chao, A. Decharon, G. Feldman, and C. Swift, 2008: The AQUARIUS/SAC-D Mission. *Oceanogr.,* 21, 68-81.

Lyzenga, D. R., 2006: Comparison of WindSat brightness temperature with two-scale model prediction. *IEEE Trans. Geosci. Rem. Sens.*, 44, 549-559.

Phillips, O. M., 1984: On the response of short ocean wave components at a fixed wavenumber to ocean current variations. *J. Phys. Oceanogr.*, 14, 1425-1433.

Phillips, O. M., 1985: Spectral and statistical properties of the equilibrium range in wind-generated gravity waves. *J. Fluid Mech.*, 156, 505-531.

Plant, W. J., 2002: stochastic, multiscale model of microwave backscatter from the ocean. *J. Geophys. Res.*, 107, C93120, doi:10.1029/2001JC000909.

Reul, N., and B. Chapron, 2001: SMOS- Salinity Data Processing Study: Improvements in emissivity models. *IFREMER* (*Institut français de recherche pour l'exploitation de la mer*) Tech. Rep. WP 1100, 130 pp.

Reul, N., and B. Chapron, 2003: A simple algorithm for sea surface salinity retrieval from L-band radiometric measurements at nadir. *Proc. Int. Geos. Remote Sens. Symp.*, *4*, 2783-2785.

Sasaki, Y., I. Asanuma, K. Muneyama, G. Naito, and T. Suzuki, 1987: The dependence of sea-surface microwave emission on wind speed, frequency, incidence angle, and polarization over the frequency range from 1 to 40 GHz. *IEEE Trans. Geosci. Rem. Sens.*, 25, 138-146.

Swift, C. T., 1974: Microwave radiometer measurements of the Cape Cod Canal. *Radio Sci.*, 9, 641-653.

Vandemark, D., B. Chapron, J. Sun, G. H. Crescenti, H. C. Graber, 2004: Ocean wave slope observations using radar backscatter and laser altimeters. *J. Phys. Oceanogr.*, 34, 2825-2842.

Walsh, E. J., D. C. Vandemark, C. A. Friehe, S. P. Burns, D. Khelif, R. N. Swift, and J. F. Scott, 1998: Measuring sea surface mean square slope with a 36-GHz scanning radar altimeter. *J. Geophys. Res.*, 103, 12587-12601.

Wentz, F. J., 1975: A two-scale scattering model for foam-free sea microwave brightness temperatures. *J. Geophys. Res.,* 80, 3441-3446.

Wentz, F. J., 1977: A two scale scattering model with application to the JONSWAP '75 aircraft microwave scatterometer experiment. *NASA Contract Rep. 2919*, 122 pp.

Yueh, S. H., 1997: Modeling of wind direction signals in polarimetric sea surface brightness temperatures. *IEEE Trans. Geosci. Rem. Sens.*, 35, 1400-1418.

Yueh, S. H., R. Kwok, F. K. Li, S. V. Nghiem, W. J. Wilson, and J. A. Kong, 1994a: Polarimetric passive remote sensing of ocean wind vectors. *Radio Sci.*, 29, 799-814.

Yueh, S. H., R. Kwok, and S. V. Nghiem, 1994b: Polarimetric scattering and emission properties of targets with reflection symmetry. *Radio Sci.*, *29*, 1409-1420.